

## MIT Open Access Articles

*Response of tropical sea surface temperature,  
precipitation, and tropical cyclone-related  
variables to changes in global and local forcing*

The MIT Faculty has made this article openly available. **Please share**  
how this access benefits you. Your story matters.

**Citation:** Emanuel, Kerry, and Adam Sobel. "Response of Tropical Sea Surface Temperature, Precipitation, and Tropical Cyclone-Related Variables to Changes in Global and Local Forcing." J. Adv. Model. Earth Syst. 5, no. 2 (June 2013): 447–458. Copyright © 2013 American Geophysical Union

**As Published:** <http://dx.doi.org/10.1002/jame.20032>

**Publisher:** American Geophysical Union (AGU)

**Persistent URL:** <http://hdl.handle.net/1721.1/85564>

**Version:** Final published version: final published article, as it appeared in a journal, conference proceedings, or other formally published context

**Terms of Use:** Article is made available in accordance with the publisher's policy and may be subject to US copyright law. Please refer to the publisher's site for terms of use.



# Response of tropical sea surface temperature, precipitation, and tropical cyclone-related variables to changes in global and local forcing

Kerry Emanuel<sup>1</sup> and Adam Sobel<sup>2</sup>

Received 10 March 2013; accepted 23 April 2013.

[1] A single-column model is used to estimate the equilibrium response of sea surface temperature (SST), precipitation, and several variables related to tropical cyclone (TC) activity to changes in both local and global forcing. Response to local forcing is estimated using the weak temperature gradient (WTG) approximation. The surface temperature is calculated using a thin slab ocean so as to maintain surface energy balance. Forcing is varied by changing the solar constant, atmospheric CO<sub>2</sub> concentration, surface wind speed, and the convergence of upper ocean heat flux. These experiments show that precipitation and variables related to TC activity are not unique functions of SST on time scales long enough for surface energy balance to be maintained. Precipitation varies inversely with SST in experiments in which the surface wind speed is varied. At low wind speed, the WTG experiments reveal a regime of high relative SST and low precipitation, which is maintained by increased transmission of longwave radiation from the surface directly to space through a dry troposphere. In general, TC potential intensity and genesis potential vary much more rapidly with SST in response to varying surface wind speed than in response to other forcings. Local changes in TC potential intensity are highly correlated with local changes in SST, showing that relative SST is a good proxy for potential intensity when forcing is strictly local, but it cannot capture potentially important changes in potential intensity that arise from global-scale changes in forcing.

**Citation:** Emanuel, K., and A. Sobel (2013), Response of tropical sea surface temperature, precipitation, and tropical cyclone-related variables to changes in global and local forcing, *J. Adv. Model. Earth Syst.*, 5, doi:10.1002/jame.20032.

## 1. Introduction

[2] Atmospheric general circulation models (AGCMs) are often used to simulate the behavior of the atmosphere, given lower boundary conditions on sea surface temperature (SST), and sometimes other surface quantities such as sea ice. The main assumption behind such simulations is that the time scale over which the atmosphere adjusts to the underlying surface is fast compared to time scales that characterize the adjustment of SST (and, e.g., sea ice) to changing conditions, and that the SST itself determines important characteristics of the atmosphere. Such assumptions seem intuitive, and SST is a convenient variable to specify for many purposes because it is relatively well observed.

[3] On the other hand, it is far from obvious that SST is an appropriate lower boundary condition. The SST is

ultimately determined in part by what happens in the atmosphere, and specifying it risks getting the causality wrong. While the temperature of the lower boundary is clearly important for radiative transfer, surface fluxes of sensible and latent heat are significant drivers of the atmosphere. Specification of a correct SST distribution would imply a correct specification of surface fluxes if the overlying atmosphere were also held fixed in the correct state. Once the atmosphere is allowed to respond to the imposed SST, however, it can do so in such a way as to render the fluxes different from those that actually produced the SST. Some atmospheric circulation systems, such as tropical cyclones (TCs) and perhaps some portion of tropical intraseasonal variability, depend on the thermodynamic disequilibrium between tropical oceans and the overlying atmospheric boundary layer, which depends in turn on surface energy fluxes and surface wind speed, not SST per se [Emanuel, 2007].

[4] The sensitivity of tropical precipitation to perturbations in SST versus perturbations in the surface energy budget was explored recently by Kang and Held [2012]. They found that the response of precipitation in the tropics to imposed interhemispheric ocean heat transport is more constrained by the surface energy budget than by SST. This is also consistent with the

<sup>1</sup>Department of Earth, Atmospheric, and Planetary Sciences, Program in Atmospheres, Oceans, and Climate, Massachusetts Institute of Technology, Cambridge, Massachusetts, USA.

<sup>2</sup>Department of Applied Physics and Applied Mathematics, and Lamont-Doherty Earth Observatory, Columbia University, New York, USA.

idea of boundary layer quasi-equilibrium [Raymond, 1995], which suggests that precipitation is strongly related to local rates of evaporation and to large-scale vertical motion, rather than to SST per se. Localized positive SST anomalies in the tropics tend to generate positive rainfall anomalies, but the associated wind speed and radiative changes tend to be a negative feedback which would reduce the SST [e.g., Sobel and Gildor, 2003; Stephens et al., 2004; Waliser, 1996]. Because that feedback is lacking, the tropical atmospheric response to imposed SST will be substantively incorrect in some climate regimes [e.g., Wu and Kirtman, 2005, 2007]. In studies of extratropical low-frequency variability, it is well established that the atmosphere forces the ocean more than vice versa, so that specification of SST anomalies leads to excessive air-sea fluxes and overestimation of predictability [Barsugli and Battisti, 1998; Bretherton and Battisti, 2000; Sutton and Mathieu, 2002].

[5] Here we examine the equilibrium response of a single-column model, including a slab ocean, to both local and global changes in external forcing as a means of ascertaining the extent to which changing SST can serve as an adequate proxy for changes in precipitation and various thermodynamic quantities of relevance to TCs. In the following section, we describe the single-column model, including its representations of radiative and convective transfer and surface fluxes. Results are presented in section 3, followed by a discussion and summary.

## 2. Methods

[6] We use the MIT single-column model described originally in Rennó et al. [1994] and updated with a modified convection scheme as described in Emanuel and Živkovic-Rothman [1999].

[7] Radiative transfer is computed interactively using the shortwave parameterization of Fouquart and Bonnel [1980] and the longwave parameterization of Morcrette [1991]. Radiative fluxes are computed at each vertical level every 3 h using instantaneous profiles of temperature, humidity, cloud fraction and cloud water path, and a climatological distribution of ozone. For the purposes of the present paper, the cloud distributions are held fixed at the values calculated from a control run using the cloud parameterization of Bony and Emanuel [2001]. Incoming solar radiation is specified using a control value of the solar constant of  $1360 \text{ W m}^{-2}$  and averaging top-of-the-atmosphere (TOA) incoming solar radiation at  $15^\circ$  north latitude over a year. Thus there are no diurnal or seasonal cycles in the radiation. For the control experiment,  $\text{CO}_2$  concentration is fixed at 360 ppm, and concentrations of  $\text{CH}_4$ ,  $\text{N}_2\text{O}$ , CFC11, and CFC12 are fixed at 1.72 ppm, 310 ppb, 280 ppt, and 484 ppt, respectively.

[8] The convection scheme of Emanuel and Živkovic-Rothman [1999] uses a buoyancy sorting algorithm similar to that of Raymond and Blyth [1986] and represents and entire spectrum of convective clouds, from shallow, nonprecipitating cumulus to deep precipitating cumulo-

nimbus. Precipitation re-evaporates and drives an unsaturated downdraft that imports enthalpy and moisture into the subcloud layer. Re-evaporation of cloud water, resulting from entrainment of dry air, drives penetrative downdrafts within the clouds. The cloud base mass flux is continuously relaxed so as to produce near neutrality of a parcel lifted dry adiabatically, and then moist adiabatically, to the first level above its lifted condensation level. This maintains a form of boundary layer quasi-equilibrium [Raymond, 1995].

[9] Surface sensible and latent heat fluxes are calculated using conventional aerodynamic flux formulae with a constant exchange coefficient of  $1.2 \times 10^{-3}$ . A constant background wind speed of  $5 \text{ ms}^{-1}$  is used in the control experiment, but this is enhanced by a gustiness factor produced by the convection scheme.

[10] The model is run with vertical levels spaced at 25 hPa, but with greater resolution above 100 hPa. A time step of 5 min is employed.

[11] A control simulation using the aforementioned standard forcing values is initialized using a tropical sounding and run into a state of radiative-convective equilibrium (RCE). As with most of the simulations reported here, the precipitation in the statistical equilibrium state fluctuates with an approximate white noise frequency spectrum and an amplitude of about 0.1% of its mean value. These very small fluctuations are likely numerical artifacts. To define the equilibrium quantities, the simulations are run until statistical equilibrium is reached for at least 50 days and the output is averaged over the last 50 days. For the control run, the SST equilibrates at slightly greater than  $27^\circ\text{C}$ , with a precipitation rate of about  $3.93 \text{ mm d}^{-1}$ . The temperature profile is dry adiabatic up to 950 hPa and nearly moist adiabatic to a tropopause at 150 hPa and with a temperature of around  $-70^\circ\text{C}$ ; above this cold point, the temperature increases upward in the model's stratosphere. Figure 1 shows vertical profiles of moist static energy and convective mass fluxes in the equilibrium state.

[12] Equilibrium perturbations about this RCE control experiment are obtained by varying three external control variables: the solar constant, the atmospheric  $\text{CO}_2$  concentration, and the background surface wind speed used for the surface fluxes. A fourth set of experiments uses specified, fixed SSTs without varying the external forcing variables; these experiments do not maintain surface energy balance and are done for comparison with the other three sets in which surface energy balance is maintained. Varying SST without varying the external control parameters is equivalent to varying the convergence of ocean heat flux into the ocean mixed layer, because the ocean flux can only affect the atmosphere through SST.

[13] These four sets of experiments are repeated in a set of simulations designed to show the effects of strictly local perturbations to the same external variables. In such experiments, the surrounding atmosphere is assumed to have the temperature of the control experiment, and fast internal waves are assumed to hold the

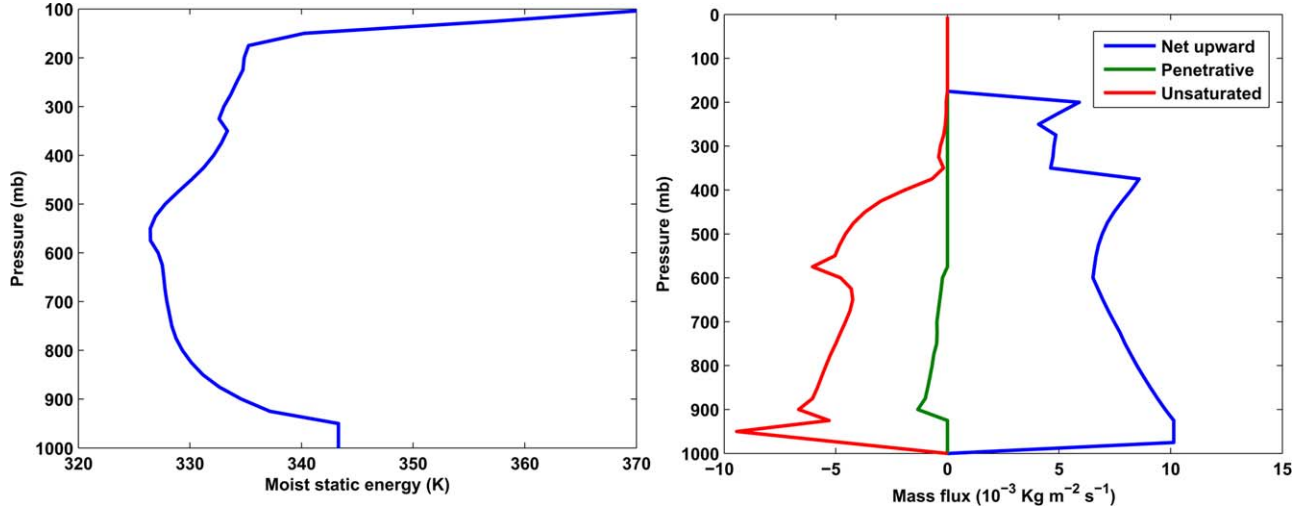


**Figure 1.** (left) Vertical profiles of moist static energy and (right) convective mass fluxes at equilibrium in the control simulation. The convective mass fluxes are composed of buoyant updrafts (blue), penetrative downdrafts (green), and a precipitation-driven unsaturated downdraft (red).

temperature fixed at its environmental value above a turbulent boundary layer. A vertical velocity is calculated at each model level such that the temperature tendency produced by vertical entropy advection balances the sum of the convective and radiative tendencies. This vertical velocity advects water vapor. (Horizontal advection of water vapor is neglected, which amounts to an assumption that the surrounding atmosphere’s water vapor profile remains equal to that of the simulated column as the latter varies. Assuming instead that the moisture profile of the surrounding atmosphere remains constant, e.g., at that of the control simulation, would modestly reduce the response to local forcing.) This weak temperature gradient (WTG) method, based on longstanding dynamical reasoning [e.g., *Charney, 1963; Held and Hoskins, 1985*] and used earlier in many idealized studies [e.g., *Clement and Seager, 1999; Miller, 1997; Neelin and Held, 1987; Pierrehumbert, 1995*] was first advanced in the context of a single-column numerical model by *Sobel and Bretherton [2000]* and has been used extensively since in understanding the response of the tropical atmosphere to relatively small-scale SST perturbations, as well as to surface wind speed perturbations over fixed SST [e.g., *Daleu et al., 2012; Kuang, 2012; Raymond, 2007; Raymond and Zeng, 2005; Romps, 2012; Sessions et al., 2010; Shaevitz and Sobel, 2004; Sobel et al., 2007; Wang and Sobel, 2011; Zhu and Sobel, 2012*]. *Chiang and Sobel [2002]* used the WTG approximation with a slab ocean to estimate the effects of El Niño-southern oscillation-induced anomalies of free tropospheric temperature on remote SST and precipitation. Here we hold the large-scale tropical atmosphere fixed and examine the response of a local ocean-atmosphere column to local changes in forcing. *Ramsay and Sobel [2011]* compared WTG single-column integrations forced by SST to RCE integrations, both forced by imposed SST, using essentially the same model as that used here. Our fixed-SST integrations are similar

to theirs, but our study differs in its use of a slab ocean and focuses on the coupled response.

[14] In addition to tabulating changes in SST and precipitation, we calculate two variables of relevance to TCs: The potential intensity, and  $\chi$ , a nondimensional measure of the thermodynamic resistance of the atmosphere to the formation of TCs [*Emanuel, 1995*]. The latter is defined

$$\chi \equiv \frac{h^* - h_m}{h_0^* - h^*}, \quad (1)$$

where  $h^*$  is the saturation moist static energy of the free troposphere (nearly constant with altitude in a moist adiabatic atmosphere),  $h_m$  is a representative value of the actual moist static energy of the middle troposphere, and  $h_0^*$  is the saturation moist static energy of the sea surface. For the present purpose, we use the minimum value of the moist static energy in the profile as a representation of  $h_m$ . We calculate potential intensity using the algorithm of *Bister and Emanuel [2002]*.

[15] Finally, given values of the potential intensity,  $V_{pot}$ , and  $\chi$ , we can calculate the thermodynamic component of an empirical genesis index. Several such indices have been developed that empirically relate observed tropical cyclogenesis rates to environmental variables thought to be important in controlling TC climatology [e.g., *Emanuel and Nolan, 2004; Gray, 1979*]. Here we use the genesis potential index (GPI) developed by *Emanuel [2010]*:

$$GPI \equiv |\eta|^3 \chi^{-4/3} \text{MAX}((V_{pot} - 35 \text{ ms}^{-1}), 0)^2 \times (25 \text{ ms}^{-1} + V_{shear})^{-4}, \quad (2)$$

where  $\eta$  is the absolute vorticity of the 850 hPa flow,  $V_{pot}$  is the potential intensity in  $\text{ms}^{-1}$ ,  $V_{shear}$  is the



magnitude of the 850–250 hPa wind shear (in  $\text{ms}^{-1}$ ), and  $\chi$  is defined by (1). As we cannot simulate the kinematic components with a single-column model, we approximate the GPI by its thermodynamic components:

$$GPI \simeq \chi^{-4/3} \text{MAX}((V_{pot} - 35 \text{ ms}^{-1}), 0)^2. \quad (3)$$

### 3. Results

#### 3.1. Response to Global Forcing

[16] Figure 2 graphs the equilibrium results of the aforementioned experiments against SST which, for three of the four sets of experiments, is calculated, not specified. We graph the results against SST to make the point that the other variables (precipitation, potential intensity,  $\chi$ , and GPI) are not identical functions of SST in equilibrium. To create Figure 2, we varied the background surface wind speed from its control value of  $5 \text{ ms}^{-1}$  down to  $1 \text{ ms}^{-1}$ , the  $\text{CO}_2$  content from its control

value of 360 ppm by successive doublings up to 11,520 ppm, the solar constant from its control value of  $1360 \text{ Wm}^{-2}$  up to  $1500 \text{ Wm}^{-2}$ , and, in the case of the specified SST experiments, from the control equilibrium value of  $27.09^\circ\text{C}$  up to  $37.09^\circ\text{C}$ . The net surface energy flux in these specified SST experiments ranges from 0 in the control case to nearly  $24 \text{ Wm}^{-2}$  for the case in which the SST is increased to  $37.09^\circ\text{C}$ . (This is also the TOA energy imbalance, as the atmosphere as a whole reaches energy equilibrium in all cases.) Thus, the climate sensitivity of this model is about  $0.4 \text{ KW}^{-1} \text{ m}^2$ , fairly consistent with other estimates of tropical climate sensitivity.

[17] Increasing the solar constant or  $\text{CO}_2$  concentration increases both the SST and the equilibrium precipitation rate (Figure 2a). Increasing the solar constant results both directly in an increased shortwave radiative flux into the ocean, and indirectly – because the atmosphere warms and water vapor therefore increases – in an increased infrared flux. This must be balanced by added turbulent enthalpy flux out of the ocean, which

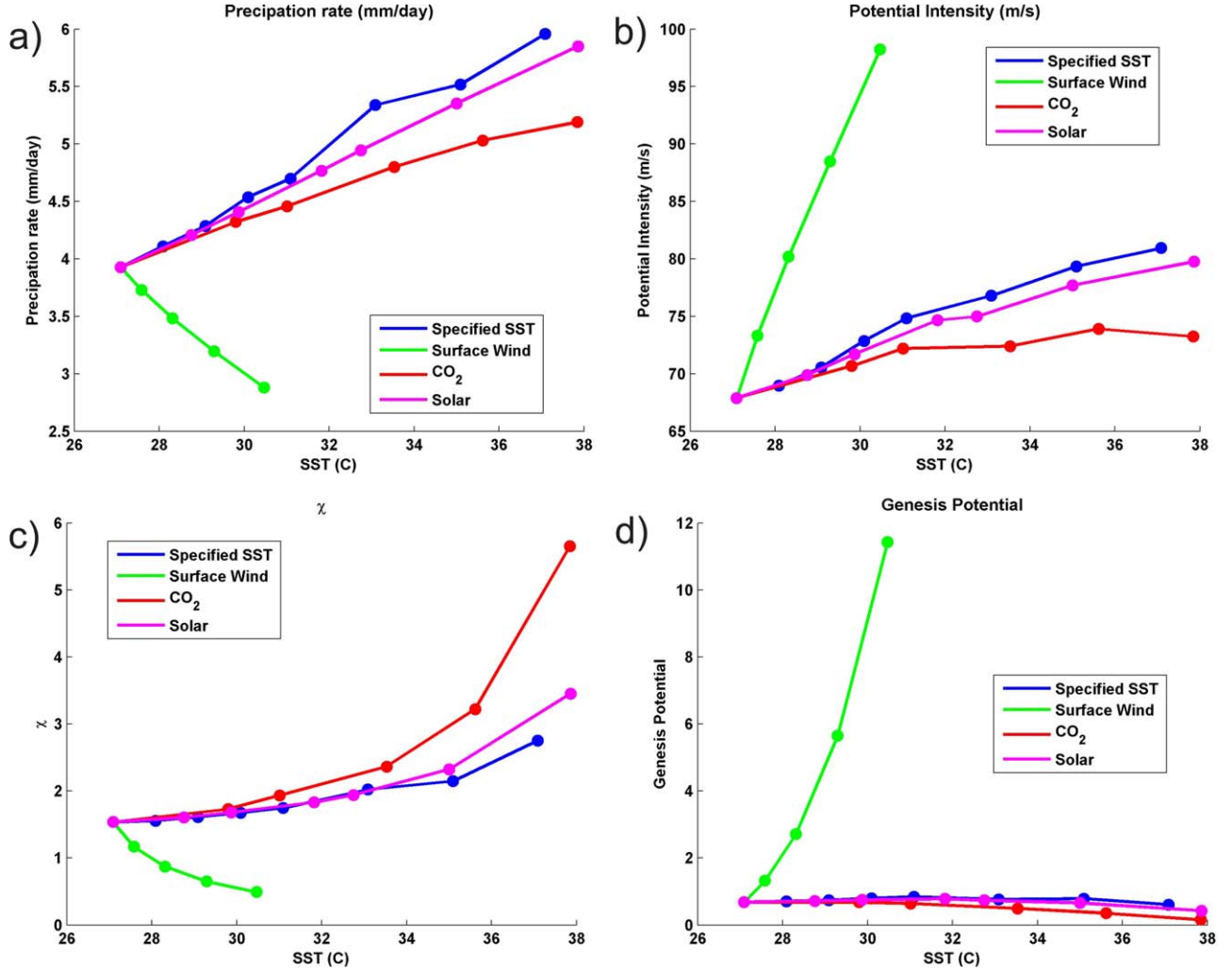


**Figure 2.** (a) Precipitation, (b) potential intensity, (c)  $\chi$ , and (d) GPI plotted against SST whose variation is specified (blue), or forced by changing surface wind (green),  $\text{CO}_2$  concentration (red), and solar constant (magenta). In the last three cases, the surface energy budget is balanced.

at these temperatures is mostly in the form of an increased latent heat flux. Hence precipitation increases. The increase with  $\text{CO}_2$  concentration is slower because the net upward infrared flux from the sea surface is already small at tropical SSTs; in fact, at sufficiently high temperature the infrared flux approaches zero and no further increase in surface enthalpy flux can occur unless the surface sensible heat flux becomes negative [O’Gorman and Schneider, 2008; Pierrehumbert, 2002]. When this happens, the boundary layer ceases to be convectively driven, and further increases in surface fluxes are problematic.

[18] It is interesting that the increase in precipitation with specified SST is slightly faster than with equilibrium SST driven by increasing insolation. This is probably owing to some absorption of solar radiation in the atmosphere, mostly by water vapor; this decreases the net radiative cooling of the cloud-bearing layer, thus reducing the latent heating (precipitation) required to balance the cooling.

[19] As an aside, note that increasing the surface temperature by adding  $\text{CO}_2$  (going up the red curve in Figure 2a), and then bringing the SST back to its control value by reducing incoming solar radiation (going down a curve parallel to the magenta curve in Figure 2a) will result in a reduction of surface precipitation relative to the control. This illustrates that compensating for  $\text{CO}_2$  increases by managing solar radiation results in a global reduction of precipitation, as is observed after major volcanic eruptions [Trenberth and Dai, 2007]; a similar reduction due to natural solar variations may have occurred during the Medieval warm period [Liu et al., 2013].

[20] Note in Figure 2a that increases in SST brought about by decreasing surface wind speed are associated with decreasing precipitation. The negative slope of the precipitation-SST curve corresponds to a decreasing latent heat flux of  $10 \text{ W m}^{-2} \text{ K}^{-1}$ , identical to the value derived by Betts and Ridgway [1989]. As wind speed is reduced, the difference between the saturation enthalpy of the sea surface and the actual enthalpy of the boundary layer must increase to maintain approximately the same turbulent enthalpy flux out of the ocean. If this were accomplished only by increasing SST, with no change in the atmosphere, then there would be an increase in TOA outgoing longwave flux because some infrared radiation emitted by the sea surface escapes to space. To compensate for this, there must be a reduced outgoing infrared flux from the atmosphere, implying a cooler atmosphere. This also results in a reduced downward infrared flux to the sea surface, thereby reducing evaporation.

[21] The behavior of potential intensity with changing forcing can be understood by noting its dependence on surface wind speed and surface radiative forcing when the surface is assumed to be in energy balance, as first derived by Emanuel [2007]:

$$V_{pot}^2 = \frac{T_s - T_o}{T_o} \frac{F_{net\downarrow} + F_{ocean}}{C_D \rho |\mathbf{V}|}, \quad (4)$$

where  $T_s$  is the SST,  $T_o$  is the outflow temperature,  $F_{net\downarrow}$  is the net radiative flux into the ocean,  $F_{ocean}$  is the convergence of heat flux within the ocean mixed layer,  $C_D$  is the surface drag coefficient,  $\rho$  is the surface air density, and  $|\mathbf{V}|$  is the surface wind speed. This relation results from combining an expression for potential intensity with one for surface energy balance.

[22] Decreasing wind speed must increase the air-sea enthalpy jump, as noted above, and this greatly increases TC potential intensity (Figure 2b) as also evident in (4). The rate of increase is about  $10 \text{ ms}^{-1} \text{ K}^{-1}$ . By contrast, increasing  $\text{CO}_2$  concentration produces a much smaller rate of increase of potential intensity with SST, and this saturates at an SST of around  $32^\circ\text{C}$  in these simulations, well before precipitation asymptotes to its solar limit. There are two reasons for this. First, potential intensity is also sensitive to outflow temperature (approximately the cold point tropopause temperature), and this increases modestly with increasing  $\text{CO}_2$  content in these simulations, partially offsetting the increase in the surface enthalpy jump. More importantly, precipitation can continue to increase somewhat after the net surface longwave flux vanishes because the sensible heat flux continues to decrease, compensated by an increased latent heat flux. In contrast, potential intensity depends on the net enthalpy flux (at constant surface wind speed), which cannot continue to increase once the surface longwave flux vanishes.

[23] Increasing the solar constant results in a continuous increase in potential intensity (Figure 2b) with an initial slope of about  $1.4 \text{ ms}^{-1} \text{ K}^{-1}$ . (From (4), this slope also depends on the surface and outflow temperatures, and sensitively on the surface wind speed.) As with precipitation, increasing SST without changing the forcing gives a larger slope than that caused by increasing insolation, and for the same reason: direct absorption of solar radiation in the atmosphere partially offsets the longwave radiative cooling, reducing the required surface enthalpy flux.

[24] The dramatically different slopes of the potential intensity-SST curves in Figure 2b suggest that global climate change may affect potential intensity principally through changing distributions of surface winds, rather than directly through surface radiative effects. In addition, changing ozone concentrations and changing distributions of the Brewer-Dobson circulation may appreciably affect outflow temperature and thereby affect potential intensity [Emanuel et al., 2013]; neither of these processes is represented in the present simulations.

[25] As the temperature of the free atmosphere increases, the thermodynamic inhibition to TCs ( $\chi$ , as given by (1)) generally increases for the reasons discussed in Emanuel et al. [2008]: Assuming that the relative humidity is nearly invariant with climate, increasing temperature increases the numerator of (1) in proportion to the saturation specific humidity in the middle troposphere, which in turn varies according to the Clausius-Clapeyron relation. On the other hand, the denominator of (1) increases more slowly with temperature as it is constrained by surface energy balance. Thus  $\chi$  increases with atmospheric temperature, and this is readily apparent in

Figure 2c. In the case of increasing  $\text{CO}_2$  concentration, the denominator of (1) saturates at SSTs not much warmer than at present, while the numerator continues to increase with temperature, yielding a large increase in  $\chi$ . Increasing insolation, on the other hand, increases the denominator of (1) continuously, yielding smaller increases of  $\chi$ . These increases are underestimated when increasing SST is specified in the absence of changes in forcing. When the surface wind speed is reduced, the atmosphere cools, for the reasons noted above, and the surface enthalpy jump increases; both of these contribute to a reduction in  $\chi$ .

[26] The thermodynamic contributions to GPI, given by (3), are displayed in Figure 2d; this depends on both  $\chi$  and potential intensity. The increasing thermodynamic inhibition to TCs ( $\chi$ ) when  $\text{CO}_2$  or insolation increases dominates the behavior of the GPI, leading to decreasing genesis potential with SST, especially when  $\text{CO}_2$  is increased. This decrease is underestimated by increasing SST without accompanying changes in the forcing. The decrease in GPI is consistent with many GCM-based calculations which generally show decreasing TC frequency with global warming [Knutson *et al.*, 2010]. But decreasing background surface wind leads to increasing SST and dramatically increasing GPI, both because  $\chi$  decreases and because potential intensity increases. This suggests that changing tropical surface wind speeds may dominate changing TC activity with climate; TCs may be thought of as a response of the climate system to weak surface winds. This may help explain why some GCMs predict increasing GPI and genesis frequency with global warming (K. Emanuel, Increased global tropical cyclone activity from global warming: Results of downscaling CMIP5 climate models, submitted to *Proceedings of the National Academy of Sciences*, 2013).

### 3.2. Response to Local Forcing

[27] When the forcing is strictly local, the local response will result in an atmospheric circulation that in turn modifies the response, mostly by changing the distribution of water vapor and clouds. In the tropics, where the Coriolis parameter is small, the circulation acts to keep the (virtual) temperature of the column the same as that of the large-scale environment, provided the column width is small compared to the deformation radius. A convenient way to represent the effects of such a circulation in the framework of a single-column model is to assume that the (virtual) temperature in the free atmosphere does not respond to changing local forcing and then to calculate the vertical velocity necessary to maintain stationarity of the (virtual) temperature. This vertical velocity is then allowed to advect water vapor (and other tracers, if applicable). We use this method (the WTG method) here, but approximate the virtual temperature by the actual temperature. We hold the temperature fixed at and above 850 hPa and calculate the vertical velocity needed to maintain the temperature. As with the global forcing experiments, we vary surface wind speed, insolation, and  $\text{CO}_2$  concentration. (Varying  $\text{CO}_2$  locally is, of course, unrealistic

but the results of doing so are nevertheless instructive.) We also perform a set of experiments in which the SST is externally specified, which is equivalent to specifying an ocean heat flux convergence. As with the global experiments, the specified SST experiments do not maintain surface energy balance.

[28] In the experiments reported on here, the solar constant is varied from 1200 to  $1500 \text{ Wm}^{-2}$ ,  $\text{CO}_2$  concentration is varied from 90 ppm by a series of doublings to 11,520 ppm, and background wind speed is varied from 1 to  $8 \text{ ms}^{-1}$ . For the set of experiments in which the local SST is specified, the relative SST (SST minus its control value) is varied from  $-3$  to  $+4 \text{ K}$ . This results in a net upward TOA radiative flux that varies from 40 to  $-14 \text{ Wm}^{-2}$ , and a net upward surface energy flux that is positive for all specified SSTs except for the control experiment value (Figure 3). The existence of positive TOA fluxes for negative specified SST anomalies may seem surprising, as one would expect an artificially cold ocean to require a heat sink rather than a source. This is related to multiple equilibria in WTG models [Sessions *et al.*, 2010]; in this case, the subsidence that results from enforcing an SST lower than the original equilibrium value dries out the column, leading to smaller downward infrared emissions to the surface. If the WTG version of our single-column model were initialized in this state, and the SST calculated, it would cool further. The TOA radiative flux behavior in the fixed SST experiments (Figure 3) is also somewhat counterintuitive: elevated SST leads to a net downward TOA radiative flux while depressed SST brings about a net emission to space. Note that the net energy source to the atmosphere that occurs in all but the coldest specified SST case is balanced by an advective export of energy. In the case of negative specified SST anomalies (except for the coldest value), this export is accomplished by a circulation in which air descends through the column, implying that the gross moist stability is negative [Sessions *et al.*, 2010].

[29] The steady-state precipitation, potential intensity,  $\chi$ , and GPI are plotted against steady-state SST (relative to the control experiment value) in Figure 4. Precipitation rates (Figure 4a) fall to zero at the three lowest values of insolation and specified SST. In these cases, strong subsidence stabilizes the atmosphere to convection, and atmospheric water vapor vanishes above the boundary layer, as there is no convective source to balance subsidence drying. For positive forcing, the rates of change of precipitation with respect to SST are much larger in magnitude than the corresponding rates when the forcing is global (Figure 2), owing to the feedback of the atmospheric circulation. Thus, for example, a positive insolation anomaly increases surface evaporation and induces an atmospheric circulation that imports water into the column; both these responses increase precipitation. Decreasing surface background wind speed yields increasing SST and decreasing precipitation, as in the global case, but the slope of the precipitation versus SST curve is larger in magnitude owing again to the feedback of the atmospheric circulation.



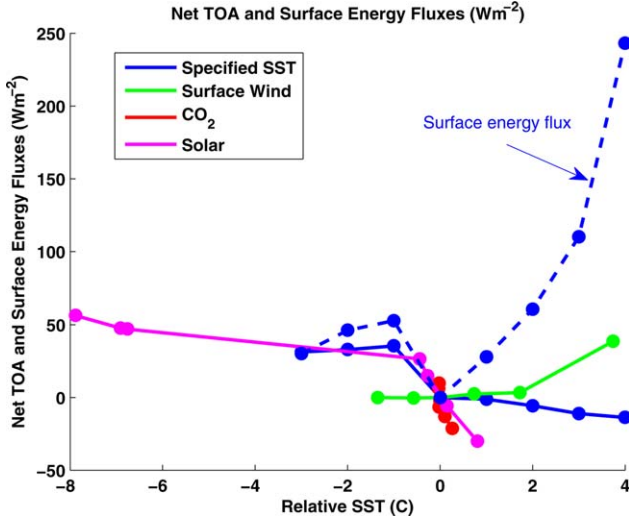


**Figure 3.** Net TOA radiative flux (solid) and surface energy flux (dashed). Changes in relative SST are specified (blue), or forced by changing local surface wind (green), local  $\text{CO}_2$  concentration (red), and local insolation (magenta). In the last three cases, the surface energy budget is balanced.

[30] The potential intensity varies with relative SST with an almost universal functional dependence (Figure 4b). This is because potential intensity variations are dominated by variations in the enthalpy jump between the surface and the boundary layer. As long as the atmosphere is undergoing deep convection, the boundary layer enthalpy is nearly equal to the saturation moist static energy of the free troposphere, which is in turn just a function of its temperature. The latter is fixed in these WTG experiments, so that potential intensity is just a (nonlinear) function of relative SST as long as there is deep convection. (The nonlinearity results from both the fact that, through Clausius-Clapeyron, the surface saturation enthalpy varies nonlinearly with SST, and the fact that the potential intensity, when expressed as a wind speed, varies with the square root of the surface enthalpy jump.) The small departures from a universal function evident in Figure 4b result from different dependencies of outflow temperature on the nature of the forcing.

[31] Note that the positive values of relative SST in Figure 4 vary over a somewhat smaller range than those in Figure 2. This is because even small positive relative SST anomalies require very large inputs of energy to the ocean if they are to be maintained in a steady state. For example, it takes  $240 \text{ Wm}^{-2}$  of ocean heat flux convergence to maintain a relative SST anomaly of 4 K (Figure 3), from which we may infer that realistic positive ocean heat flux convergence can produce only small positive departures of SST from its background state. (On the other hand, it takes much less of an energy sink to create negative relative SST anomalies once the boundary layer becomes convectively decoupled from the free troposphere, which likely explains the well-known negative skewness of the distribution of tropical SST; e.g., *Sobel et al.* [2002], *Wallace* [1992])

As with the global forcing case, decreasing background surface wind is effective in increasing potential intensity, but the slope of the potential intensity versus SST curve brought about by changing surface winds in the locally forced case is only about half that of the globally forced solution.

[32] Although the concept of relative SST is unambiguous in the present study, its appropriate definition in the real world is far from obvious. *Swanson* [2008] and many subsequent papers define it as the local SST relative to a tropical mean SST. But averaging SST over the entire tropics will include, for example, the east Pacific cold tongue, which is usually convectively decoupled from the free troposphere, so it is doubtful whether these cold SSTs have much relationship to the mean tropospheric temperature. Moreover, surface energy fluxes from tropical land masses contribute significantly to the overall energy balance, and these are excluded when considering relative SST. The difference between the saturation entropy based on the local SST and that of the tropical mean atmospheric temperature at some reference level in the upper troposphere, such as 300 hPa, would avoid these ambiguities while still presumably behaving similarly to relative SST [e.g., *Johnson and Xie*, 2010].

[33] The behavior of the thermodynamic resistance to TCs, as represented by  $\chi$ , is opposite to that of the global solutions, for positive forcing. Globally, holding relative humidity fixed as the climate changes is usually a good approximation, but this is not the case with positive local SST anomalies, which induce upward motion, which in turn moistens the column. This works in the opposite sense of increasing temperature per se, decreasing the numerator of (1), while increasing surface enthalpy jump increases the denominator; both act to reduce  $\chi$ .

[34] Because  $\chi$  decreases and potential intensity increases for increasing positive forcing, the GPI also increases with the forcing, giving a nearly universal GPI-relative SST function for small positive perturbations in relative SST. But it must be borne in mind that it takes a very large local energy source to increase relative SST appreciably, except when the SST increase is brought about by decreasing background surface wind speed. Once again, decreasing surface wind emerges as a primary candidate for increasing TC activity.

[35] As the response to wind speed is qualitatively different from the response to other forcings, it is of some interest to analyze it in greater detail. Particularly interesting are the dynamics maintaining the state of high relative SST and low precipitation that occurs at the lowest value of wind speed. The steady state budget of column-integrated moist static energy is a useful diagnostic. It can be combined with the dry static energy budget to form a relation for the precipitation [e.g., *Sobel*, 2007; *Wang and Sobel*, 2011]:

$$P = (1/M) (E + H - R) + R - H, \quad (5)$$

where  $E$  and  $H$  are the latent and sensible heat fluxes, respectively,  $R$  is column-integrated radiative cooling



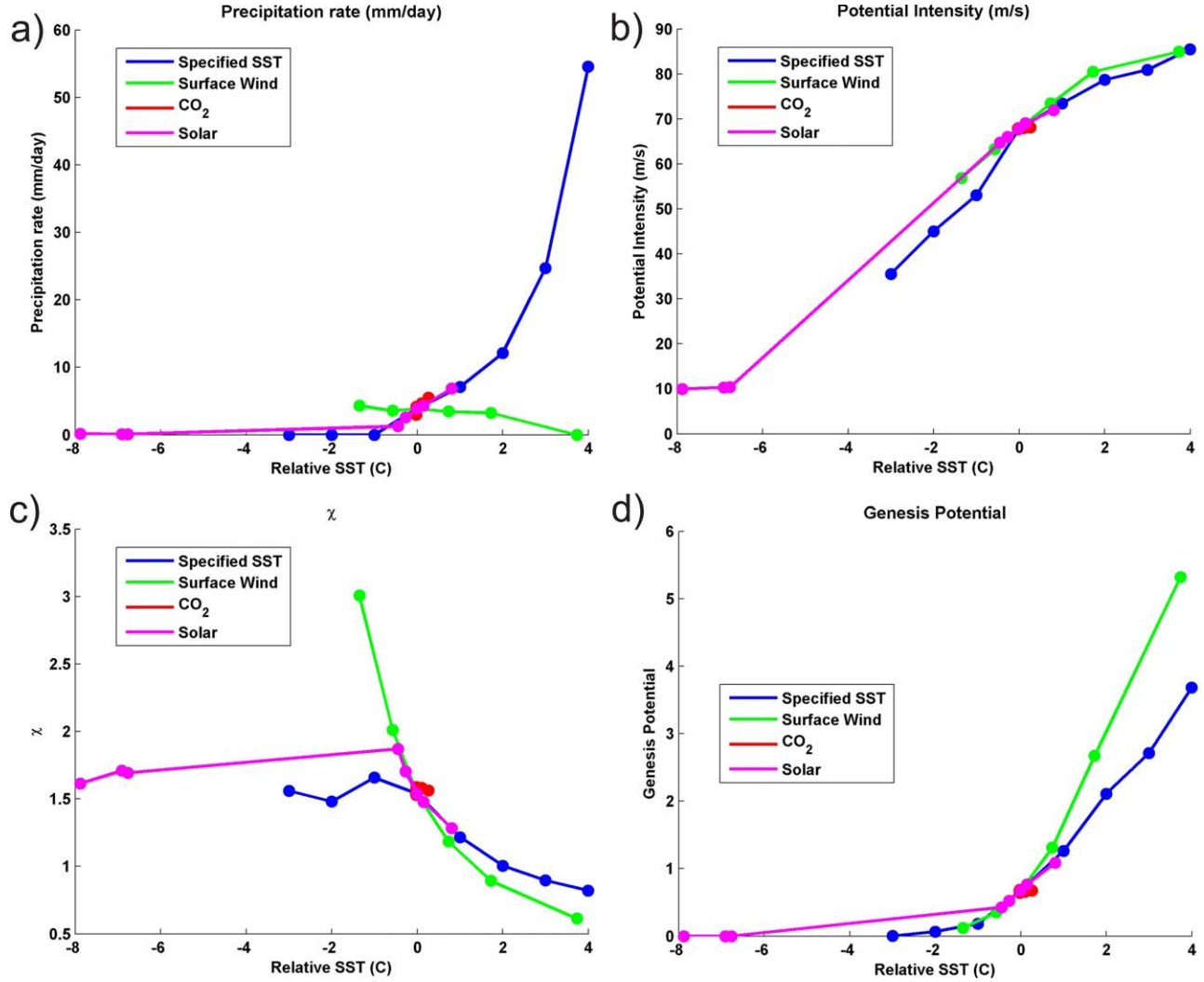


**Figure 4.** (a) Precipitation, (b) potential intensity, (c)  $\chi$ , and (d) GPI plotted against SST relative to that of the control experiment. Changes in relative SST are specified (blue), or forced by changing local surface wind (green), local CO<sub>2</sub> concentration (red), and local insolation (magenta). In the last three cases, the surface energy budget is balanced.

(difference between TOA and surface radiative fluxes, defined positive if TOA flux exceeds surface flux),  $M$  is the normalized gross moist stability [e.g., *Raymond et al.*, 2009], and all quantities are expressed in energy units. The first term on the right-hand side (RHS) represents implied advective energy export out of the column (if positive; import if negative) which causes deviations from RCE. In an RCE state, this reduces to a balance in the dry static energy budget between latent heating, radiative heating, and surface sensible heat flux,  $P - R + H = 0$ .

[36] Figures 5 and 6 show respectively  $R$  and the net implied energy import  $-(1/M)(E + H - R)$  versus SST for the experiments forced by varying surface wind speed, while Figure 7 shows the net turbulent surface energy fluxes together with the TOA and surface radiative fluxes from the same experiments. We see from Figure 5 that the column radiative cooling decreases gradually with SST (note the scale on the y axis); Figure

7 reveals that this is due to an increase in the net surface radiative flux, due presumably to the SST increase, which exceeds the change in the TOA radiative flux. At the same time, the turbulent flux decreases with SST, as it must to maintain surface energy balance. Except for the highest value of SST, the net energy import is approximately constant with SST, due to compensation between these two, with the normalized gross moist stability  $M$  apparently remaining approximately constant as well.

[37] Between the two lowest values of wind speed (two highest values of SST), however, there is a qualitative change in the physics. The surface radiative flux increases more rapidly than it did with SST than it did for lower SST. The surface latent heat flux compensates with a more rapid decrease as it must to maintain surface energy balance. However, the TOA radiative flux, which had remained approximately constant with SST at lower SST, now increases approximately in step with

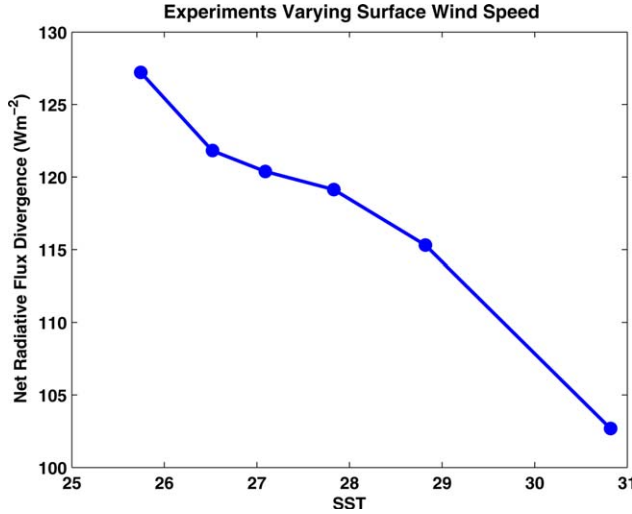


**Figure 5.** Column-integrated radiative cooling, plotted against SST for the WTG experiments forced by surface wind speed.

the surface radiative flux, so that the column radiative cooling does not increase as fast as the surface radiative flux increases. This means that the total surface turbulent flux decreases more than the column radiative cooling does. The normalized gross moist stability does not change enough to compensate, so that the energy import rapidly increases (first term on the RHS of (5) becomes more negative), consistent with a decrease in  $P$ .

[38] The matching between the surface and TOA radiative flux increases can be interpreted as an increased transmission of longwave radiative energy directly from the surface to space. This occurs because the atmosphere dries out in response to large-scale descent which becomes strong at the highest SST values. This in turn is consistent with the shutdown of condensation as pre-

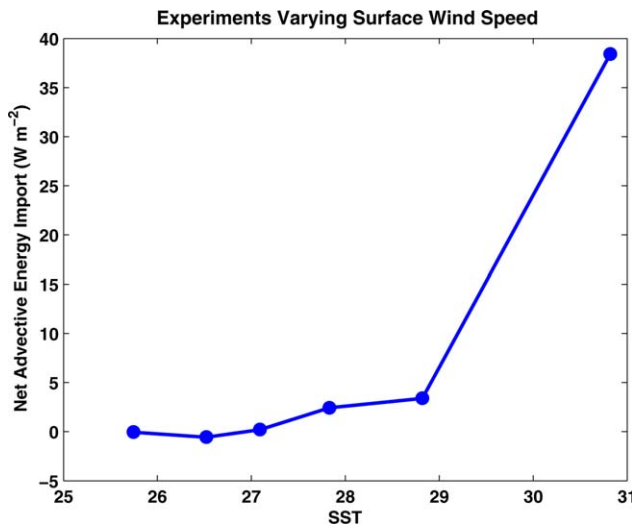


**Figure 6.** Net implied advective energy import, plotted against SST for the WTG experiments forced by surface wind speed.

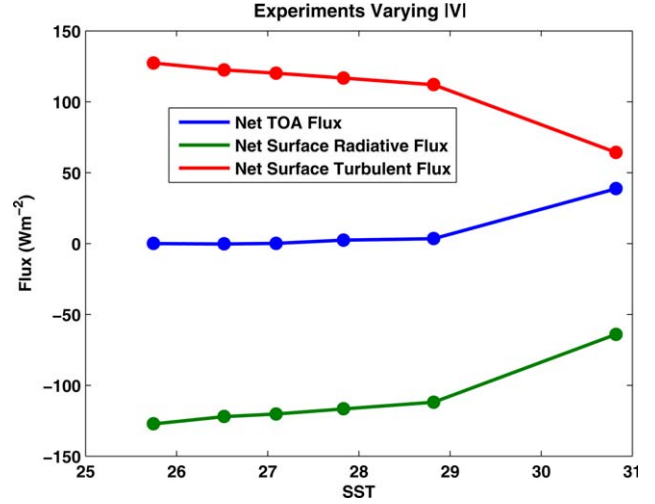


**Figure 7.** Net TOA radiative flux, net surface radiative flux, and net surface turbulent flux, plotted against SST for the WTG experiments forced by surface wind speed.

cipitation becomes small, so that adiabatic warming associated with descent must balance radiative cooling on its own. Figures 8 and 9 show the profiles of pressure vertical velocity and relative humidity as functions of SST and pressure. The onset of strong descent and a dry column are apparent at the highest SST.

[39] It has long been observed that the highest SST values often occur simultaneously with small or zero precipitation [e.g., Waliser *et al.*, 1993]. While this defies expectation if one believes that SST (even relative SST) controls precipitation under all circumstances, it is readily understood when one thinks about the behavior of the coupled system. In our simulations, this is explicitly clear, as the surface wind speed is the control parameter. We find it of interest to see explicitly the physics that allows this to be maintained in a steady state. Horizontal moisture advection would add some

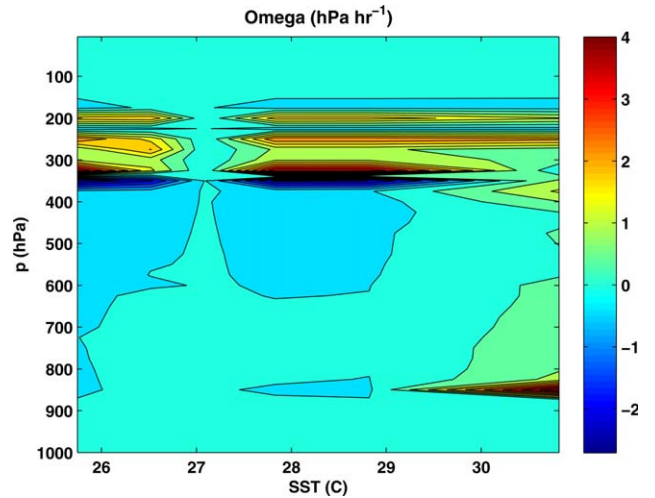


**Figure 8.** Pressure vertical velocity plotted against SST and pressure, for the WTG experiments forced by surface wind speed.

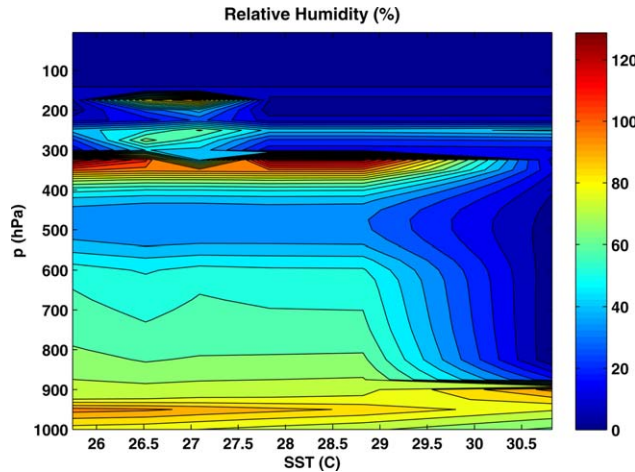


**Figure 9.** Relative humidity plotted against SST and pressure, for the WTG experiments forced by surface wind speed.

complexity in the real atmosphere; nonetheless, the simple picture found here may be relevant to places of high SST and low precipitation. These may include the Arabian Sea, some portions of the west Pacific warm pool, and others, including locations experiencing strong suppressed phases of the Madden-Julian oscillation.

#### 4. Summary and Discussion

[40] SST is often considered an appropriate boundary condition for the general circulation of the atmosphere, and AGCMs are often run with SST and a few other quantities, such as sea ice, specified as boundary conditions. Such models often produce reasonable facsimiles of the actual climate system, in terms of broad features of the general circulation [e.g., *Compo et al.*, 2011]. But specification of the SST in the absence of a correct specification of the environmental factors (e.g., surface winds, clouds, greenhouse gas concentrations, and insolation) can lead to potentially large imbalances in the surface energy budget, which are associated with anomalous surface fluxes and anomalous air-sea thermodynamic disequilibrium. This will lead to errors in precipitation and in the susceptibility of the system to TCs. Suppose, for example, that a  $1^{\circ}\text{C}$  positive SST anomaly arises in nature from locally weak surface winds, but that an AGCM run with specified SST fails, for whatever reason, to produce the light wind anomaly associated with the positive SST anomaly. Given the results of the previous section, the AGCM will produce, in this case, a positive precipitation anomaly, where in reality a negative precipitation anomaly exists, and will underestimate the susceptibility of the region to TC formation. A  $1^{\circ}\text{C}$  positive SST anomaly, absent the wind anomaly that produced it, will be associated with a surface energy flux anomaly of about  $60 \text{ W m}^{-2}$ . For tropical precipitation, as pointed out by *Kang and Held* [2012], and for TC-related thermodynamic parameters, it is essential to have correct surface fluxes and (independently) correct surface wind speeds; merely having a

correct SST distribution is not enough, and may not be as important as having correct surface fluxes and surface wind speeds.

[41] A body of empirical work [e.g., *Emanuel*, 2005; *Knutson et al.*, 2010; *Swanson*, 2008; *Vecchi and Soden*, 2007] suggests that various measures of TC activity can be related to some function of the SST distribution, ranging from local SST to combinations of local and remote SST. But the present work shows that TC potential intensity and genesis potential cannot be uniquely related to any function of SST, except that potential intensity has a simple universal relationship to strictly local SST anomalies regardless of the cause of the latter. But relative SST cannot capture potentially important changes in potential intensity brought about, for example, by changes in surface wind speeds that affect a large fraction of the tropical ocean surface, such as might be expected from a weakening of the global tropical circulation [e.g., *Vecchi et al.*, 2006].

[42] Changes in the SST and atmospheric state that occur in response to wind speed are qualitatively different from those in response to the other forcing variables. In the case of local forcing, our simulations illuminate the physics of a regime at low wind speeds in which SST is large but precipitation and humidity are small. This regime does not exist in simulations using fixed SST as a lower boundary condition. In this regime, the low column humidity allows increased transmission of longwave radiation directly from the surface to space, so that column radiative cooling does not decrease as rapidly as surface turbulent flux (which must balance the surface radiative flux) does. The moist and dry static energy budgets then require an advective energy import; this occurs as a result of descent in the presence of a positive gross moist stability. The descent at the same time maintains the dryness of the atmospheric column.

[43] The relatively weak dependence of TC potential intensity on global  $\text{CO}_2$  concentration, at least for the relative high-control value of surface wind used here, suggests that global warming effects on TCs primarily operate indirectly, through changes in surface wind, ocean heat fluxes, and clouds and water vapor. Although not considered here, changes in vertical wind shear are also known to have an important influence on TC activity.

[44] An alternative approach to specifying SST in AGCMs is to use a slab ocean layer with specified lateral heat fluxes [e.g., *Sutton and Mathieu*, 2002] or specified ocean currents that transport calculated temperature [Winton, 2003]. In such approaches, SST is not constrained to have any particular distribution, and while there is no guarantee that surface energy fluxes will be correct, wildly anomalous fluxes are far less likely than with specified SST. Whether SSTs are specified or a slab ocean approach is used, incorrect surface wind speeds can result in substantial errors in TC potential intensity; thus attention should be paid to surface wind speed (independent of surface fluxes) in evaluating all GCMs.



[45] **Acknowledgments.** The first author was supported by NSF grant AGS-0850639, and the second by NSF grant AGS-1008847.

## References

- Barsugli, J. J., and D. S. Battisti (1998), The basic effects of atmosphere-ocean thermal coupling on midlatitude variability, *J. Atmos. Sci.*, **55**, 477–493.
- Betts, A. K., and W. Ridgway (1989), Climatic equilibrium of the atmospheric convective boundary layer over a tropical ocean, *J. Atmos. Sci.*, **46**, 2621–2641.
- Bister, M., and K. A. Emanuel (2002), Low frequency variability of tropical cyclone potential intensity: 1. Interannual to interdecadal variability, *J. Geophys. Res.*, **107**(D24), 4801, doi:10.1029/2001JD000776.
- Bony, S., and K. A. Emanuel (2001), A parameterization of the cloudiness associated with cumulus convection: Evaluation using TOGA COARE data, *J. Atmos. Sci.*, **58**, 3158–3183.
- Bretherton, C. S., and D. S. Battisti (2000), An interpretation of the results from atmospheric general circulation models forced by the time history of the observed sea surface temperature distribution, *Geophys. Res. Lett.*, **27**, 767–770.
- Charney, J. G. (1963), A note on large-scale motions in the tropics, *J. Atmos. Sci.*, **20**, 607–608.
- Chiang, J. C. H., and A. H. Sobel (2002), Tropical tropospheric temperature variations caused by ENSO and their influence on the remote tropical climate, *J. Clim.*, **15**, 2616–2631.
- Clement, A. C., and R. Seager (1999), Climate and the tropical oceans, *J. Clim.*, **12**(12), 3383–3401.
- Compo, G. P., et al. (2011), The twentieth century reanalysis project, *Q. J. R. Meteorol. Soc.*, **137**, 1–28.
- Daleu, C., S. Woolnough, and R. Plant (2012), Cloud-resolving model simulations with one and two-way couplings via the weak-temperature gradient approximation, *J. Atmos. Sci.*, **69**, 3683–3699.
- Emanuel, K. (2005), Increasing destructiveness of tropical cyclones over the past 30 years, *Nature*, **436**, 686–688.
- Emanuel, K. (2007), Environmental factors affecting tropical cyclone power dissipation, *J. Clim.*, **20**, 5497–5509.
- Emanuel, K. (2010), Tropical cyclone activity downscaled from NOAA-CIRES reanalysis, 1908–1958, *J. Adv. Model. Earth Syst.*, **2**, 1–12. doi:10.3894/JAMES.2010.2.1.
- Emanuel, K., R. Sundararajan, and J. Williams (2008), Hurricanes and global warming: Results from downscaling IPCC AR4 simulations, *Bull. Am. Meteorol. Soc.*, **89**, 347–367.
- Emanuel, K., S. Solomon, and D. Folini (2013), Influence of tropopause transition layer cooling on Atlantic hurricane activity, *J. Clim.*, **26**, 2288–2301.
- Emanuel, K. A. (1995), The behavior of a simple hurricane model using a convective scheme based on subcloud-layer entropy equilibrium, *J. Atmos. Sci.*, **52**, 3959–3968.
- Emanuel, K. A., and D. S. Nolan (2004), Tropical cyclone activity and the global climate system, paper presented at 26th AMS Conference on Hurricanes and Tropical Meteorology, Am. Meteorol. Soc., Miami.
- Emanuel, K. A., and M. Živkovic-Rothman (1999), Development and evaluation of a convection scheme for use in climate models, *J. Atmos. Sci.*, **56**, 1766–1782.
- Fouquart, Y., and B. Bonnel (1980), Computation of solar heating of the Earth's atmosphere: A new parameterization, *Beitr. Phys. Atmos.*, **53**, 35–62.
- Gray, W. M. (1979), *Hurricanes: Their formation, structure, and likely role in the tropical circulation*, in *Meteorology Over the Tropical Oceans*, edited by D. B. Shaw, pp. 155–218, R. Meteorol. Soc., J. Glazier House, Grenville Place, Bracknell, Berkshire, United Kingdom.
- Held, I. M., and B. J. Hoskins (1985), Large-scale eddies and the general circulation of the troposphere, *Adv. Geophys.*, **28**, 3–31.
- Johnson, N. C., and S.-P. Xie (2010), Changes in the sea surface temperature threshold for tropical convection, *Nat. Geosci.*, **3**, 842–845.
- Kang, S. M., and I. M. Held (2012), Tropical precipitation, SSTs and the surface energy budget: A zonally symmetric perspective, *Clim. Dyn.*, **38**, 1917–1924.
- Knutson, T. R., J. L. McBride, J. Chan, K. Emanuel, G. Holland, C. Landsea, I. Held, J. P. Kossin, A. K. Srivastava, and M. Sugi (2010), Tropical cyclones and climate change, *Nature Geosci.*, **3**, 157–163.
- Kuang, Z. (2012), Weakly forced mock-Walker cells, *J. Atmos. Sci.*, **69**, 2759–2786.
- Liu, J., B. Wang, M. A. Cane, S.-Y. Yim, and J.-Y. Lee (2013), Divergent global precipitation changes induced by natural versus anthropogenic forcing, *Nature*, **493**, 656–659.
- Miller, R. L. (1997), Tropical thermostats and low cloud cover, *J. Clim.*, **10**(3), 409–440.
- Morcrette, J.-J. (1991), Radiation and cloud radiative properties in the European centre for medium-range weather forecasts forecasting system, *J. Geophys. Res.*, **96**, 9121–9132.
- Neelin, J. D., and I. M. Held (1987), Modeling tropical convergence based on the moist static energy budget, *Mon. Weather Rev.*, **115**, 3–12.
- O’Gorman, P. A., and T. Schneider (2008), The hydrological cycle over a wide range of climates simulated with an idealized GCM, *J. Clim.*, **21**, 3815–3832.
- Pierrehumbert, R. T. (1995), Thermostats, radiator fins, and the local runaway greenhouse, *J. Atmos. Sci.*, **52**, 1784–1806.
- Pierrehumbert, R. T. (2002), The hydrologic cycle in deep-time climate problems, *Nature*, **419**, 191–198.
- Ramsay, H. A., and A. H. Sobel (2011), Effects of relative and absolute sea surface temperature on tropical cyclone potential intensity using a single-column model, *J. Clim.*, **24**, 183–193.
- Raymond, D. J. (1995), Regulation of moist convection over the west Pacific warm pool, *J. Atmos. Sci.*, **52**, 3945–3959.
- Raymond, D. J. (2007), Testing a cumulus parameterization with a cumulus ensemble model in weak temperature gradient mode, *Q. J. R. Meteorol. Soc.*, **133**, 1073–1085.
- Raymond, D. J., and A. M. Blyth (1986), A stochastic model for nonprecipitating cumulus clouds, *J. Atmos. Sci.*, **43**, 2708–2718.
- Raymond, D. J., and X. Zeng (2005), Modelling tropical atmospheric convection in the context of the weak temperature gradient approximation, *Q. J. R. Meteorol. Soc.*, **131**, 1301–1320.
- Raymond, D. J., S. L. Sessions, and A. H. Sobel (2009), The mechanics of gross moist stability, *J. Adv. Model. Earth Syst.*, **1**, 9, doi:10.3894/JAMES.2009.1.9.
- Rennó, N. O., K. A. Emanuel, and P. H. Stone (1994), Radiative-convective model with an explicit hydrological cycle: Part I. Formulation and sensitivity to model parameters, *J. Geophys. Res.*, **99**, 14,429–14,441.
- Romps, D. M. (2012), Numerical tests of the weak pressure gradient approximation, *J. Atmos. Sci.*, **69**, 2846–2856.
- Sessions, S. L., S. Sugaya, D. J. Raymond, and A. H. Sobel (2010), Multiple equilibria in a cloud-resolving model using the weak temperature gradient approximation, *J. Geophys. Res.*, **115**, D12110, doi:10.1029/2009JD013376.
- Shaevitz, D. A., and A. H. Sobel (2004), Implementing the weak temperature gradient approximation with full vertical structure, *Mon. Weather Rev.*, **132**(2), 662–669.
- Sobel, A. H. (2007), Simple models of ensemble-averaged precipitation and surface wind, given the SST, in *The Global Circulation of the Atmosphere*, edited by T. Schneider and A. H. Sobel, Princeton Univ. Press, Princeton, N. J.
- Sobel, A. H., and C. S. Bretherton (2000), Modeling tropical precipitation in a single column, *J. Clim.*, **13**, 4378–4392.
- Sobel, A. H., and H. Gildor (2003), A simple time-dependent model of SST hot spots, *J. Clim.*, **16**, 3978–3992.
- Sobel, A. H., I. M. Held, and C. S. Bretherton (2002), The ENSO signal in tropical tropospheric temperature, *J. Clim.*, **15**, 2702–2706.
- Sobel, A. H., G. Bellon, and J. T. Bacmeister (2007), Multiple equilibria in a single-column model of the tropical atmosphere, *Geophys. Res. Lett.*, **34**, L22804, doi:10.1029/2007GL031320.
- Stephens, G. L., P. J. Webster, R. H. Johnson, R. Engelen, and T. L’Ecuyer (2004), Observational evidence for the mutual regulation of the tropical hydrological cycle and tropical sea surface temperatures, *J. Clim.*, **17**, 2213–2224.
- Sutton, R., and P.-P. Mathieu (2002), Response of the atmosphere-ocean mixed-layer system to anomalous ocean heat-flux convergence, *Q. J. R. Meteorol. Soc.*, **128**, 1259–1275.



- Swanson, K. (2008), Nonlocality of Atlantic tropical cyclone intensities, *Geochem. Geophys. Geosyst.*, *9*, Q04V01, doi:10.1029/2007GC001844.
- Trenberth, K. E., and A. Dai (2007), Effects of Mount Pinatubo volcanic eruption on the hydrological cycle as an analog of geoengineering, *Geophys. Res. Lett.*, *34*, L15702, doi:10.1029/2007GL030524.
- Vecchi, G. A., and B. J. Soden (2007), Effect of remote sea surface temperature change on tropical cyclone potential intensity, *Nature*, *450*, 1066–1070.
- Vecchi, G. A., B. J. Soden, A. T. Wittenberg, I. M. Held, A. Leetma, and M. J. Harrison (2006), Weakening of tropical Pacific atmospheric circulation due to anthropogenic forcing, *Nature*, *441*, 73–76.
- Waliser, D. E. (1996), Formation and limiting mechanisms for very high sea surface temperature: Linking the dynamics and the thermodynamics, *J. Clim.*, *9*, 161–188.
- Waliser, D. E., N. E. Graham, and C. Gautier (1993), Comparison of the highly reflective cloud and outgoing longwave radiation datasets for use in estimating deep convection, *J. Clim.*, *6*, 331–353.
- Wallace, J. M. (1992), Effect of deep convection on the regulation of tropical sea surface temperature, *Nature*, *357*, 230–231.
- Wang, S., and A. H. Sobel (2011), Response of convection to relative sea surface temperature: Cloud-resolving simulations in two and three dimensions, *J. Geophys. Res.*, *116*, D11119, doi:10.1029/2010JD015347.
- Winton, M. (2003), On the climatic impact of ocean circulation, *J. Clim.*, *16*, 2875–2889.
- Wu, R., and B. P. Kirtman (2005), Roles of Indian and Pacific ocean air-sea coupling in tropical atmospheric variability, *Clim. Dyn.*, *25*, 155–170.
- Wu, R., and B. P. Kirtman (2007), Regimes of seasonal air-sea interaction and implications for performance of forced simulations, *Clim. Dyn.*, *29*, 393–410.
- Zhu, H., and A. H. Sobel (2012), Comparison of a single column model in weak temperature gradient mode to its parent AGCM, *Q. J. R. Meteorol. Soc.*, *138*, 1025–1034.

---

Corresponding author: K. Emanuel, Program in Atmospheres, Oceans, and Climate, Massachusetts Institute of Technology, Cambridge, MA 02139, USA. (emanuel@mit.edu)